8-2020

Embedding parallelohedra into primitive cubic networks and structural automata description

Mikhail M. Bouniaev
The University of Texas Rio Grande Valley

Sergey V. Krivovichev

Recommended Citation

Bouniaev, M. M., and S. V. Krivovichev. 2020. "Embedding Parallelohedra into Primitive Cubic Networks and Structural Automata Description." Acta Crystallographica Section A: Foundations and Advances 76 (6): 698–712. https://doi.org/10.1107/S2053273320011663.

Acta Cryst A FOUNDATIONS ADVANCES

ISSN 2053-2733

Embedding parallelohedra into primitive cubic networks and structural automata description

Mikhail M. Bouniaev[a]* and Sergey V. Krivovichev[b,c]

[a]School of Mathematical and Statistical Sciences, University of Texas Rio Grande Valley, One University Boulevard, Brownsville, TX 78520, USA, [b]Kola Science Centre, Russian Academy of Sciences, Fersmana Str. 14, Apatity 184209, Russian Federation, and [c]Department of Crystallography, St Petersburg State University, University Emb. 7/9, St Petersburg 199034, Russian Federation. *Correspondence e-mail: mikhail.bouniaev@utrgv.edu

Received 9 March 2020
Accepted 25 August 2020

Edited by U. Grimm, The Open University, UK

Keywords: parallelohedra; crystalline structures; primitive cubic nets; deterministic finite automata; structural automata.

The main goal of the paper is to contribute to the agenda of developing an algorithmic model for crystallization and measuring the complexity of crystals by constructing embeddings of 3D parallelohedra into a primitive cubic network (**pcu** net). It is proved that any parallelohedron P as well as tiling by P, except the rhombic dodecahedron, can be embedded into the 3D **pcu** net. It is proved that for the rhombic dodecahedron embedding into the 3D **pcu** net does not exist; however, embedding into the 4D **pcu** net exists. The question of how many ways the embedding of a parallelohedron can be constructed is answered. For each parallelohedron, the deterministic finite automaton is developed which models the growth of the crystalline structure with the same combinatorial type as the given parallelohedron.

1. Introduction

The overarching goal of this paper is to contribute to the agenda of developing a model for crystal growth (crystallization) and methodology to measure crystal complexity through deterministic finite automata (DFA). The problem of crystallization is one of the fundamental and difficult problems of crystallography. The geometric approach for modeling crystalline structures is a local theory of regular systems that was developed by B. N. Delone, his associates and followers (Delone *et al.*, 1976; Dolbilin, 1976; Dolbilin & Schattschneider, 1998; Schattschneider & Dolbilin, 1998; Baburin *et al.*, 2018). Though significant progress has been made in developing the local theory, rigorously proven results have not yet been used by practicing crystallographers.

To some extent, the theory of DFA, particularly cellular automata (CA) and structural automata (SA), may complement the local theory and narrow the gap between mathematical theory and crystallography in the area of crystal growth. CA and SA are instruments to model crystallization as the result of attaching given blocks to each other according to certain rules. The crystal growth is thus viewed as a dynamic periodic process that can be described using an algorithm consisting of a finite number of steps. Each step corresponds to the attachment of a certain structure element (atom, molecule, fundamental building block *etc.*) to the already existing structure. Since the algorithm is finite, it can be modeled by means of DFA which can be analyzed within the framework of corresponding branches of computer science. The crystallization is therefore considered as computation.

The basic idea of the approach is to model in terms of DFA the growth of periodic orthogonal nets, *i.e.* nets that can be obtained from a primitive cubic network (**pcu** net) by

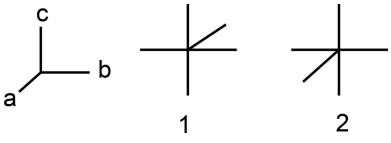

eliminating portions of its vertices and/or edges. The advantage of orthogonal nets lies in their simplicity and relatively easy visualization. Though by far not all crystal structures can be described as based upon orthogonal nets, they are of the utmost importance for crystal chemistry (Krivovichev, 2014*a*). As was shown by Alexandrov *et al.* (2011), more than 75% of all known metal–organic frameworks are based on ten types of nets: **dia**, **pcu**, **srs**, **ths**, **cds**, **lvt-a**, **pts**, **nbo**, **utp** and **mog**. All these nets are orthogonal by direct descent, *i.e.* can be obtained from the **pcu** net by the elimination of some vertices and edges. In mineralogy, the most important rock-forming minerals such as quartz, feldspars and feldspathoids are based upon orthogonal nets of different topologies and complexities. Among all known zeolite framework types, about half are based upon orthogonal nets and may be obtained by linkage of blocks with orthogonal topologies. Many layered materials, *e.g.* oxysalts and 2D coordination polymers, are based upon 2D orthogonal nets (Krivovichev, 2009).

The SA that were used to model the growth of orthogonal nets by Krivovichev *et al.* (2012), Krivovichev (2014*a*) are the modified versions of the crystal lattice automata first suggested by Morey *et al.* (2002) for educational purposes. The SA approach provides a relatively easy and transparent tool to model the growth of orthogonal nets and to estimate their complexities by counting the number of states in the corresponding DFA. This measure may be viewed as reflecting an algorithmic (dynamic) complexity in contrast to informational (static) complexity, which is based on the application of the Shannon information theory (Krivovichev, 2012, 2014*b*; Hornfeck, 2020).

The idea of using finite automata (and in particular CA) in the study of crystals and their growth has a long history. As far as we know, it was first suggested by Alan Mackay (1976) and since then used by many authors to investigate structures and their defects (Krivovichev, 2004; Crutchfield, 2012; Varn *et al.*, 2013*a*,*b* *etc.*). The algorithmic approach to the growth of crystals has many parallels with modern approaches to self-assembly (Cartwright & Mackay, 2012) and molecular computing (see, *e.g.*, Adar *et al.*, 2004).

The basic problem in the theory of orthogonal nets is the evaluation of conditions for a specific net to be orthogonal. From the mathematical point of view, this problem is equivalent to the question of whether a given net can be embedded into the **pcu** net. The idea of this work is to develop a basic methodology for the solution of this problem through a systematic study of basic periodic structures, namely, tiling of the 3D Euclidean space ($\mathbb{R}^3$) by parallelohedra in the context of embedding them into the **pcu** net and modeling by SA. To be more precise, we study edge graphs of parallelohedra and edge graphs of tilings by parallelohedra and show that they can be embedded into the edge graph of the **pcu** net.

One of the innovative approaches of this work is that though we develop SA that model 3D structures, we suggest utilizing as a hosting **pcu** net not only the 3D **pcu** net, but also the **pcu** net of an arbitrary dimension n (nD **pcu** net). As we show, the 3D **pcu** net is 'tight' even for the rhombic dodecahedron, *i.e.* the rhombic dodecahedron cannot be embedded into the 3D **pcu** net though the crystal's graph satisfies some evident necessary conditions which reflect properties of the 3D **pcu** net, *i.e.* the degree of any vertex in the graph must not exceed 6, and the graph must not contain cycles with an odd number of edges. It is also worth noting that the higher the degree of vertices of the graph to be embedded into the nD **pcu** net, the higher the dimension n of the hosting nD **pcu** net must be.

One more thing we would like to draw attention to is that, in this paper, not only are embeddings of parallelohedra (and tilings by parallelohedra) into the **pcu** net constructed, but we also answer the question of how many ways the embedding of a parallelohedron can be constructed. The corresponding statements are directly related to the capability of the automaton to reproduce a periodic structure. To the best of our knowledge, the general conditions under which SA uniquely reproduce a space structure that is embedded into the nD **pcu** net and under what conditions the structure is periodic are not known.

To conclude the *Introduction*, we will outline the content of the paper. In the second section, the main objects of our study are briefly introduced: parallelohedra, nD **pcu** net and related concepts. In the third section, the main theorems about embedding of parallelohedra and tiling by parallelohedra are proved. In the fourth section, the concepts of DFA and SA as an example of DFA are introduced. For the tiling of $\mathbb{R}^3$ by a parallelohedron, the SA is constructed as a model for the growth of a structure that has the combinatorial type of the given parallelohedron.

Our review of parallelohedra is based on the work of Dolbilin (2012), and we follow Krivovichev (2014*a*) in the review of the concepts of DFA, SA and 3D **pcu** net.

This work grew out of the talk presented by S. Krivovichev at the workshop 'Soft Packings, Nested Clusters and Condensed Matter' held at the American Institute of Mathematics (AIM) in San Jose, California, USA, 19–23 September, 2016. It is the result of collaboration between a crystallographer (SK) and a mathematician (MB), with an important input from N. P. Dolbilin and M. M. Stogrin, which explains its style, where we attempt to combine mathematical rigor with crystallographic intuition.

2. Parallelohedra, pcu networks and related concepts

2.1. Parallelohedra and tiling in $\mathbb{R}^3$

Parallelohedra play an important role in mathematics. They can be considered a model for fundamental cells in $\mathbb{R}^3$ and, therefore, are also important in crystallography, chemistry and physics. The concept, as well as the term, parallelohedron were introduced by E. S. Fedorov (1885). He discovered all five combinatorial types of parallelohedra (Fig. 1), namely, cube, hexagonal prism, elongated dodecahedron, rhombic dodecahedron and truncated octahedron, called by Coxeter (1973) 'primary' parallelohedra. The term parallelohedron reflects the fact that if it is possible to tile (see the definition below) a

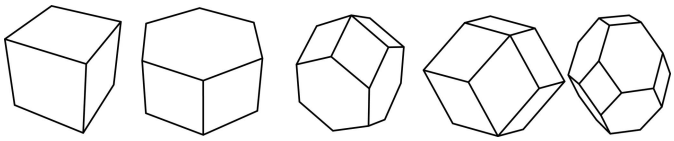

Figure 1
Five Fedorov parallelohedra: cube, hexagonal prism, elongated dodecahedron, rhombic dodecahedron, truncated octahedron.

space with parallel copies of a polyhedron, then any of its faces have an equal opposite parallel face.

Definition 2.1. Let **T** be a set of convex polyhedra $P_1, \ldots, P_n \ldots$ placed in $\mathbb{R}^d$ such that interior points of any two polyhedra do not overlap, and the union of polyhedra is equal to $\mathbb{R}^d$. Then, the set **T** is called a tiling, and elements P_i are called cells or tiles of tiling.

Definition 2.2. Assume $P_1, \ldots, P_n \ldots$ is a tiling for $\mathbb{R}^d$. It is called a face-to-face tiling if any two tiles that have a non-empty intersection intersect by the entire face for both polyhedra of dimension k $(0 \leq k \leq d-1)$.

Definition 2.3. A parallelohedron of dimension d is defined as a closed convex d-dimensional polyhedron P in $\mathbb{R}^d$ such that the set of parallel copies of P is a tiling for $\mathbb{R}^d$, *i.e.* there is a tiling $P_1, \ldots, P_n \ldots$ where each P_i can be obtained as the result of the parallel shift of P. This tiling will be called a tiling by parallelohedron P.

In this paper, we will consider only face-to-face tilings by parallelohedra.

Remark 2.1. (i) Face-to-face tiling **T** by the parallelohedron P is uniquely defined by the parallelohedron P and its position in $\mathbb{R}^d$. (ii) Face-to-face tiling **T** by the parallelohedron P is a lattice tiling, *i.e.* there is a lattice with integer coefficients $\Lambda_P = \{\sum_1^d \lambda_i \mathbf{e}_i, \lambda_i \in \mathbb{Z}\}$, such that $\mathbf{T} = P + \Lambda_P$.

Definition 2.4. For a given parallelohedron P, the lattice Λ_P as defined above will be called a lattice of the tiling by P or just a lattice of P.

The concept of a facet vector will play a significant role in our future discussions.

Definition 2.5. Assume P is a parallelohedron with center O, **T** is a tiling by P and m is a number of hyperfaces of P. If P_i $(i = 1, \ldots, m)$ is a parallel copy of P adjacent to P by a hyperface and centered at point O_i, then the vector $\mathbf{t}_i = \vec{OO_i}$ is called a facet vector for P.

Remark 2.2. It is not hard to prove that among all facet vectors of parallelohedron P in $\mathbb{R}^3$, there are three vectors that form the basis of the lattice of P. We defined a facet vector as the vector connecting centers of adjacent parallelohedra; however, it is more convenient to find it by connecting corresponding vertices of parallel hyperfaces.

The Minkovski theorem (Minkovski, 1897) as stated below is important for the theory of parallelohedra.

Theorem 2.1. If P is a d-dimensional parallelohedron, then (i) P is centrally symmetric; (ii) all hyperfaces of P are centrally symmetric.

We will end this subsection with the definition of the graph of a tiling.

Definition 2.6 (graph of a tiling). For a given parallelohedron P and the tiling of $\mathbb{R}^3$ by P, the graph of parallelohedron P (the graph of the tiling by P, respectively) is the graph whose vertices are vertices of P (all vertices of the tiling's cells, respectively). The edges of the graph are all edges of P (the union of all edges of parallel copies of P in the tiling, respectively). This graph is also called an edge graph of the parallelohedron (of the tiling, respectively).

If the tiling of $\mathbb{R}^3$ by parallelohedron P is given, then Γ_P stands for the infinite graph of the tiling as defined above. $\Phi\Gamma_P$ stands for the finite graph of P itself.

2.2. pcu networks and related definitions

An ideal orthogonal network (net) is defined as a network in $\mathbb{R}^3$ with edges of equal length and an angle between adjacent edges of 90°. Adjacent edges are defined as having only one vertex/node in common. A full ideal orthogonal network or a primitive cubic network (**pcu** net) is an ideal orthogonal network with a maximum degree (6 for $\mathbb{R}^3$) in every vertex/node (Delgado-Friedrichs *et al.*, 2003). Some examples of orthogonal nets are given in Fig. 2.

For convenience, we can always assume that the equal edge length of a **pcu** net is 1. It is usually assumed that a **pcu** net is a 3D object or a 2D object. This concept of the **pcu** net as a 3D object can be easily extended to the n-dimensional primitive cubic net (nD **pcu** net) as follows:

Definition 2.7. (nD **pcu** net). The n-dimensional primitive cubic net is defined as an n-dimensional grid or a geometric graph in $\mathbb{R}^n$ whose nodes (vertices) are all points of $\mathbb{Z}^n$, and

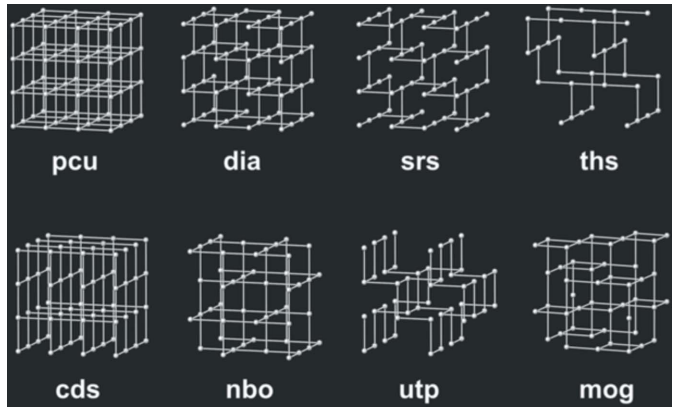

Figure 2
Examples of orthogonal nets (Krivovichev, 2014*a*).

edges are all intervals that connect nodes and have length 1. We will call the edges of the graph 'unit' edges.

If the dimension of the nD **pcu** net is not specified, it is assumed by default that $n = 3$, *i.e.* the **pcu** net stands for a traditionally defined 3D object. A unit cube in $\mathbb{Z}^n$ will also be called a unit cube cell of the nD **pcu** net.

Definition 2.8. We say that a polyhedron can be embedded into the nD **pcu** net if there is a combinatorial isomorphism of the graph of the polyhedron and a subgraph of the nD **pcu** net. We will call this isomorphism an embedding of the polyhedron into the nD **pcu** net.

We say that a tiling can be embedded into the nD **pcu** net if there is a combinatorial isomorphism of the graph of the tiling and a subgraph of the nD **pcu** net. We will call this isomorphism an embedding of the tiling into the nD **pcu** net.

Remark 2.3. (i) If a polyhedron (tiling by a polyhedron, respectively) is embedded into the nD **pcu** net, then the image (range) of the above-defined isomorphisms will also be called an embedding of the polyhedron (tiling by the polyhedron, respectively) into the nD **pcu** net. (ii) Assume we have two embeddings of a polyhedron (or tiling by a polyhedron) into the nD **pcu** net. If there is a symmetry of the nD **pcu** net that maps the range of one embedding onto the range of another embedding, we will consider them the same embeddings. (iii) If a polyhedron (or tiling by a polyhedron) is embedded into the nD **pcu** net, and we map the graph of the polyhedron (tiling by the polyhedron, respectively) by combinatorial automorphism onto itself and embed it in the same way as the original embedding, then these two embeddings will be considered the same embeddings. (iv) As was noted in Remark 2.1, tiling by a parallelohedron is a lattice tiling, *i.e.* $\mathbf{T} = P + \Lambda_P$. We will consider embeddings that 'preserve' this structure, *i.e.* if f is an embedding and $Q = P + \lambda$, then $f(Q) = f(P) + t$ for some vector t. All embeddings of parallelohedra as defined below satisfy this property.

3. Embeddings of parallelohedra into an nD pcu net

In this section, it is proved that face-to-face tiling of $\mathbb{R}^3$ by any parallelohedron, except the rhombic dodecahedron, can be embedded into the **pcu** net. We also prove that the rhombic dodecahedron cannot be embedded into the 3D **pcu** net. However, we show that the rhombic dodecahedron and tiling by it can be embedded into the 4D **pcu** net.

We prove that embedding of the hexagonal prism is unique, and both the elongated dodecahedron and truncated octahedron can be embedded in two different ways.

Remark 3.1. (i) Once the embedding of the parallelohedron P is established, the method of proof and construction of the corresponding tilings' embeddings are very similar for all parallelohedra, except the tiling by the rhombic dodecahedron. Namely, as was mentioned in Section 2, the lattice Λ_P for the parallelohedron P can be found such that $\Lambda_P + P$ is a tiling uniquely determined by the position of P. Once the embedding f of P into the **pcu** net is established, lattice $\Lambda'_{f(P)}$ can be found such that $\Lambda'_{f(P)} + f(P)$ is an embedding of a tiling by P defined by f. Basis vectors of lattice $\Lambda'_{f(P)}$ can be chosen as the images of three facet vectors that form the basis of Λ_P. (ii) Because of this observation, for the hexagonal prism and elongated dodecahedron, we only provide vectors that form bases for Λ_P and $\Lambda'_{f(P)}$ accompanied by self-explanatory pictures of the corresponding embeddings. Since both embeddings of the truncated octahedron are more complicated constructions, we discuss in greater detail the embedding of tiling for one of the embeddings ('matchbox' embedding). We also show the basis for $\Lambda'_{f(P)}$ and some fragments of the tiling for the second possible embedding ('cutout corners' embedding). Considering the observation above, these detailed discussions may not seem necessary, but we believe it will give a good understanding of how the embedding is constructed and of the edge configuration at each vertex for the corresponding SA.

Definition 3.1. For a given parallelohedron P and a given embedding f of P into the **pcu** net, lattice $\Lambda'_{f(P)}$ as defined above in Remark 3.1 will be called a lattice of the embedding of tiling by P.

We state some facts related to 4-cycles and 6-cycles in the **pcu** net that are used in proofs for parallelohedra embeddings in the form of two easy-to-prove lemmas (Lemmas 3.1 and 3.2).

Definition 3.2. Four 4-cycles in the **pcu** net C_1, C_2, C_3, C_4 will be called a 4-4 clique if they have a common vertex; C_1 has common edges with C_4 and C_2; C_i (where $i = 2, 3$) has common edges with C_{i-1} and C_{i+1}; C_4 has common edges with C_3 and C_1. The first number 4 shows that there are four cycles in the clique, the second 4 indicates that each cycle in the clique is a 4-cycle.

Lemma 3.1. (i) Any 4-cycle in the **pcu** net is a perimeter of a square face of a unit cube cell and, therefore, it always belongs to a unit cube cell. (ii) Two adjacent edges in the **pcu** net that belong to the same line cannot be the edges of the same 4-cycle. (iii) A 4-4 clique can be situated (up to orientation) in the **pcu** net only in two different patterns – either in one plane as shown in Fig. 3(*a*), or in two perpendicular planes (two cycles in each plane) as shown in Figs. 3(*b*), 3(*c*). (iv) Three 4-cycles in the **pcu** net that have exactly one common vertex and pairwise common edges can be uniquely (up to orientation) situated in the **pcu** net.

Lemma 3.2. (i) Any 6-cycle in the **pcu** net rests either in one unit cube cell, or in two unit cube cells adjacent by a common face. If it rests in two unit cube cells, then all six vertices belong to two adjacent square faces of the unit cube cells that belong to the same plane. (ii) If AB and AD are two adjacent perpendicular edges of a fixed unit cube cell in the **pcu** net,

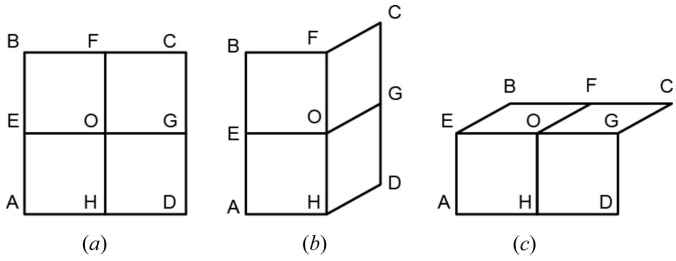

Figure 3
4-4 clique.

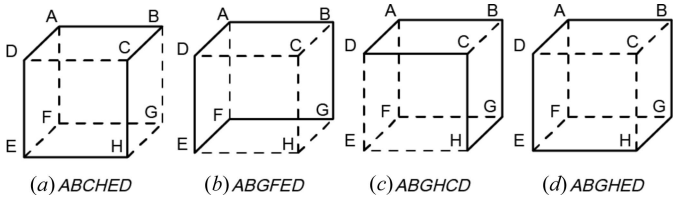

Figure 4
Embedding of a hexagon.

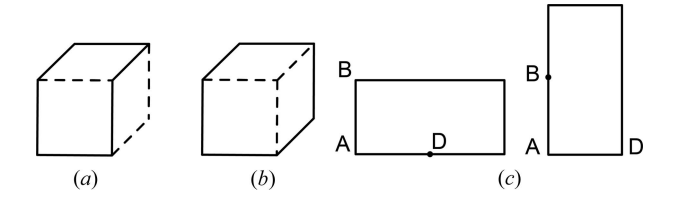

Figure 5
(*a*) Angle shape embedding, (*b*) hexagon shape embedding, (*c*) one plane embedding.

then there are four ways to design a 6-cycle with edges AB and AD such that all cycles belong to the same fixed unit cube cell (Fig. 4). (iii) If AB and AD are two adjacent perpendicular edges of a unit cube cell in the **pcu** net, then there are two different ways to design a 6-cycle with edges AB and AD such that the entire cycle does not belong to one unit cube cell [Fig. 5(*c*)]. (iv) If AB and AD are two adjacent edges of a unit cube cell in the **pcu** net that belong to the same line, then there are four ways to design a 6-cycle with edges AB and AD. Any design belongs to two unit cube cells adjacent by the square face. (v) There are only three types [listed below in Figs. 5(*a*), 5(*b*), 5(*c*)] of embeddings of the hexagon into the **pcu** net. We call the embedding as shown in Fig. 5(*a*) an 'angle shape' embedding ('angle shape' 6-cycle); as shown in Fig. 5(*b*) a 'hexagon shape' embedding ('hexagon shape' 6-cycle); and as shown in Fig. 5(*c*) a 'one plane' embedding ('one plane' 6-cycle). (vi) If AB and AD are two adjacent perpendicular edges of a unit cube cell in the **pcu** net, then there are ten different ways to design a 6-cycle with edges AB and AD: two 'one plane' cycles, two 'hexagon shape' cycles and six 'angle shape' cycles.

3.1. Embedding of a hexagonal prism into a pcu net

Theorem 3.1. The hexagonal prism can be embedded into the **pcu** net. The face-to-face tiling by the hexagonal prism can be embedded into the **pcu** net.

Proof. Assume Q is a hexagonal prism as shown in Fig. 6(*a*). Let us take a $2 \times 1 \times 1$ parallelepiped Π in the **pcu** net comprised of two adjacent unit cubes as shown in Fig. 6(*b*). All vertices A_i, B_i $(i = 1, \ldots, 6)$ and edges that connect vertices of the hexagonal prism are mapped on the corresponding vertices A_i', B_i' and corresponding edges of two adjacent unit cubes in the **pcu** net as shown in Fig. 6(*b*). The above-defined mapping is an embedding of the prism into the **pcu** net.

Let us show bases for two lattices Λ_P and $\Lambda'_{f(P)}$ (Remark 3.1) that define tiling by the hexagonal prism and embedding f of the tiling, respectively. A basis for the lattice Λ_P of the tiling can be chosen as $e_1 = \vec{A_1A_5}$, $e_2 = \vec{A_1A_3}$ and $e_3 = \vec{A_1B_1}$. Assume A_1' is the origin (0, 0, 0) in the **pcu** net [Fig. 6(*b*)], the x axis is along the edge $A_1'A_5'$, the y axis is along the edge $A_1'A_3'$ and the z axis is along the edge $A_1'B_1'$. Then vectors $e_1' = [2, 0, 0]$, $e_2' = [1, 1, 0]$ and $e_3' = [0, 0, 1]$ form the basis of the lattice $\Lambda'_{f(P)}$. In Fig. 7, we demonstrate the projection of the tiling on the plane that contains the upper base of the prism and the embedding of this projection. □

Theorem 3.2. Embedding of the hexagonal prism into the **pcu** net is uniquely defined.

Proof. As follows from Lemma 3.2 point (v), a hexagon can be embedded into the **pcu** net in three different ways (up to orientation). Using Lemmas 3.1 and 3.2, it is easy to prove that

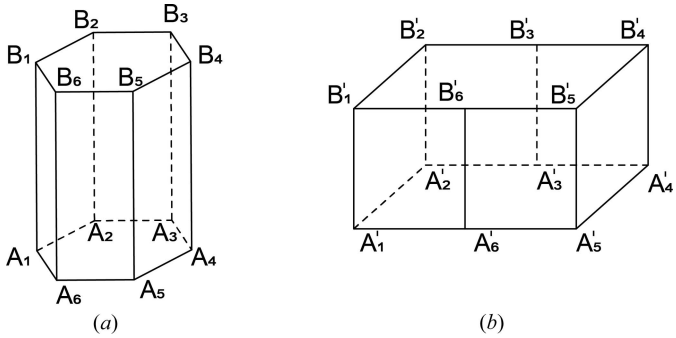

Figure 6
Embedding of a hexagonal prism.

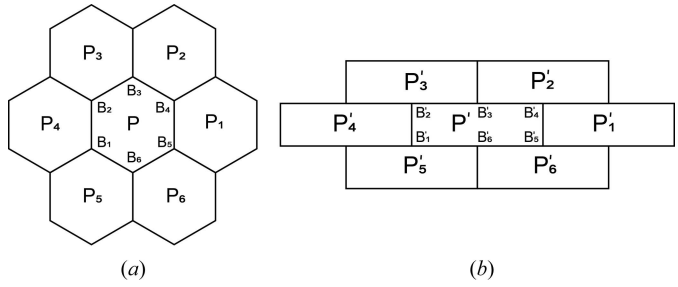

Figure 7
(*a*) Projection of a tiling by a hexagonal prism and (*b*) embedding of this projection.

if the hexagonal base is embedded as the 'angle shape' or 'hexagon shape' embedding [Lemma 3.2 point (v)], the embedding cannot be extended to the graph of the entire prism.

Therefore, the only way to embed the hexagonal base while embedding hexagonal prisms is to do it as the 'one plane' embedding. Assume we have the 'one plane' embedding $ABCDEF$ of a hexagonal base where edges AB and AF are perpendicular. Let us take the vertex A and an edge AA' of a 4-cycle adjacent to AB that is an image of the rectangular face of the prism. This edge is perpendicular to the plane of the 'one plane' embedding. When the direction of AA' is chosen, all six 4-cycles that are images of rectangular faces of the prism are uniquely defined, which, in turn, uniquely defines the second 6-cycle that is the image of the second hexagonal base of the prism. □

3.2. Embedding of an elongated dodecahedron into a pcu net

In this subsection, two methods to embed the elongated dodecahedron into the **pcu** net are designed. As follows from Lemma 3.1, a 4-4 clique can be situated (up to orientation) in the **pcu** net only in two different patterns – either in one plane or in two perpendicular planes (two 4-cycles in each plane). While embedding four rhombi faces with a common vertex of the elongated dodecahedron onto the 4-cycles that do not belong to the same plane, we can 'bend' the image in two different ways and in two different directions. The results of these 'bendings' are the same as far as the embedding is concerned (Remark 2.3).

It is also shown that the designed methods are the only possible methods to embed the elongated dodecahedron. Each of these methods can be extended to the embedding of tiling by the elongated dodecahedron.

Theorem 3.3. An elongated dodecahedron can be embedded into the **pcu** net.

Proof. Method 1. Assume $\Phi\Gamma_{\rm ED}$ is the graph of the elongated dodecahedron $GA_1 \ldots A_8B_1 \ldots B_8F$ where F and G stand for two common vertices of four rhombi as shown in Fig. 8(a) (G is not visible in the picture). Let us now take the $2 \times 2 \times 1$ parallelepiped $G'A'_1 \ldots A'_8B'_1 \ldots B'_8F'$ as shown in Fig. 8(b).

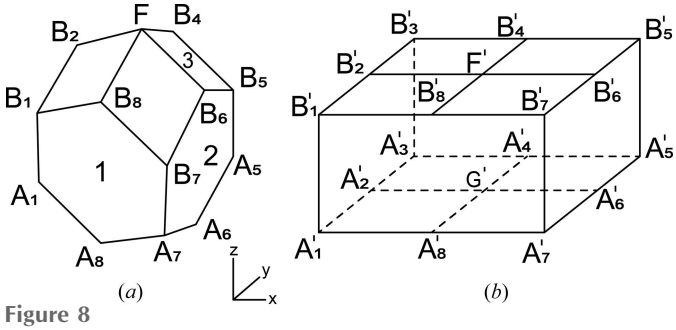

Figure 8
Embedding of an elongated dodecahedron by Method 1.

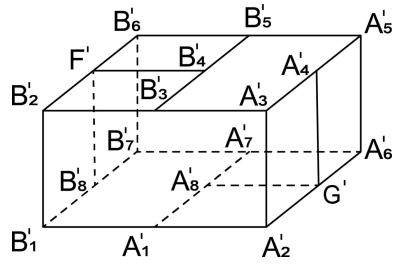

Figure 9
Embedding of an elongated dodecahedron by Method 2.

Mapping any vertex A_i, B_i ($i = 1 \ldots 8$), F, G and edges of the elongated dodecahedron onto the corresponding nodes A'_i, B'_i, F', G' and edges of the $2 \times 2 \times 1$ parallelepiped in the **pcu** net as shown in Fig. 8 establishes the required embedding.

Method 2. Embedding by the second method is shown in the self-explanatory Fig. 9. For consistency, we keep the same notations for the vertices of the elongated dodecahedron as in Method 1. □

Remark 3.2. For convenience, we use parentheses in notations for points in $\mathbb{R}^3$ and square brackets for vectors.

Theorem 3.4. Tiling by an elongated dodecahedron can be embedded into the **pcu** net.

Proof. Assume P is an elongated dodecahedron and P' is its image as designed in Theorem 3.3, Method 1 [Fig. 8(b)]. Let us introduce a system of coordinates and the origin in the **pcu** net. Assume A'_1 is the origin (0, 0, 0) [Fig. 8(b)], the x axis is along the edge $A'_1A'_7$, the y axis is along the edge $A'_1A'_3$ and the z axis is along the edge $A'_1B'_1$.

By connecting corresponding points that belong to the parallel edges in three pairs of parallel centrally symmetric faces, we find a basis for the lattice Λ_P of the elongated dodecahedron. Though not any three pairs of parallel faces can be taken to form a basis, vectors that correspond to two pairs of parallel hexagonal faces and one pair of square faces will form a basis. The following three vectors form a basis: $e_1 = \vec{A_1A_7}$ corresponds to face 1 and the face parallel to face 1 (face $\parallel$ 1), $e_2 = \vec{A_1A_3}$ (face 2 and face $\parallel$ 2) and $e_3 = \vec{A_1F}$ (face 3 and face $\parallel$ 3).

The corresponding vectors in the **pcu** net that form a basis for the lattice of the embedding of P (Definition 3.1) are e'_1 =

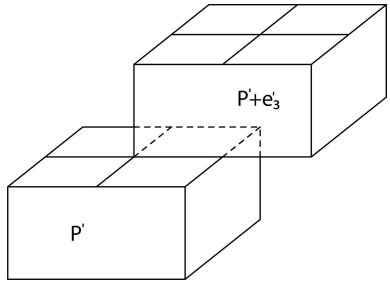

Figure 10
Embedding of an elongated dodecahedron tiling. Shift of P' by e'_3.

$[2, 0, 0]$, $e'_2 = [0, 2, 0]$ and $e'_3 = [1, 1, 1]$. Shifts of P' by all linear combinations with integer coefficients of the vectors e'_1, e'_2 and e'_3 define the embedding of tiling by P. For example, all shifts of the parallelepiped P' by the integer multiples of vector e'_1 create an infinite strip of parallelepipeds $P' + \lambda_i e'_1$ along the x axis. All shifts of the created strip by the integer multiples of vector e'_2 create one layer of parallelepipeds where the corresponding 'layer' of tiling by P is embedded. The shift of P' by e'_3 is shown in Fig. 10.

In a similar way, the embedding designed in Method 2 can be extended to the embedding of tiling by P. □

Theorem 3.5. There are only two ways to embed the elongated dodecahedron into the **pcu** net.

Proof. We use Fig. 8 and Fig. 9 as reference pictures for embedding by Method 1 and Method 2, respectively. We would like to emphasize that we do not know what the images of embeddings look like and, therefore, images of the elongated dodecahedron as shown in Fig. 8(b) and Fig. 9 cannot be used to substantiate the proof. We start with two different patterns of 4-cycle embeddings and uniquely restore both embeddings of the elongated dodecahedron. We use notations A'_i and B'_i for images of the corresponding vertices (A_i and B_i) of the embedding under consideration.

As stated in Lemma 3.1 point (ii), there are two ways to position a 4-4 clique. Hence, four rhombi faces of the elongated dodecahedron that have a common vertex F can be embedded in two ways that have to be considered separately – case 1 [Fig. 8(b)] and case 2 (Fig. 9). Since these proofs are very similar, in order to demonstrate arguments used in both, we present here only the proof of case 2 as it is more complicated compared with case 1.

Case 2. Assume that the 4-4 clique, the image of four rhombi with the common vertex F, is situated in two perpendicular planes as shown in Fig. 9. Currently, we assume that the rest of the picture, besides four 4-cycles $B'_1B'_2F'B'_8$, $B'_2F'B'_4B'_3$, $B'_8F'B'_6B'_7$ and $B'_6B'_5B'_4F'$, does not exist. Let us take two adjacent 4-cycles $B'_1B'_2F'B'_8$ and $B'_2F'B'_4B'_3$ with a common vertex F', and two perpendicular edges $B'_1B'_2$ and $B'_3B'_2$ that have a common vertex B'_2. Since B_1B_2 and B_3B_2 are edges of a hexagonal face of the elongated dodecahedron, a 6-cycle that is the image of the hexagonal face must be adjacent to two chosen 4-cycles (along edges $B'_1B'_2$ and $B'_3B'_2$). For two perpendicular edges by Lemma 3.2 [Figs. 4(a)–4(d) and Fig. 5(c)], there are ten possible ways to design a 6-cycle with these edges: two ways that result in two 'one plane' 6-cycles, and eight ways that result in a cycle that belongs to the same unit cube with the given edges.

Let us show that in the design of the elongated dodecahedron's embedding, only the first two ways are possible.

There are two adjacent unit cubes with perpendicular edges $B'_1B'_2$ and $B'_3B'_2$. Each cube contains four 'one cube' 6-cycles. First, let us consider cube $B'_1B'_2B'_3B'_4F'B'_8A'_8A'_1$ as shown in Fig. 9. Since the hexagonal face of the elongated dodecahedron does not have F as a vertex, the 6-cycle $B'_1B'_2F'B'_4B'_3A'_1$ that has F' as a vertex must be excluded from consideration. Since $B'_8A'_8$ is not an edge (B'_8 already has degree 3), two 6-cycles $B'_1B'_8A'_8A'_1B'_3B'_2$ and $B'_1B'_2B'_3B'_4A'_8B'_8$ are not possible. And, finally, since $A'_8B'_4$ is not an edge (B'_4 already has degree 3), the cycle $B'_1B'_2B'_3B'_4A'_8A'_1$ is not possible.

Let us consider now four possible ways to design a 6-cycle in the second unit cube that is adjacent to the cube $B'_1B'_2B'_3B'_4F'B'_8A'_8A'_1$ and has two common perpendicular edges $B'_1B'_2$ and $B'_3B'_2$ with it.

Following the order of Figs. 4(a)–4(d), we construct four 'one cube' 6-cycles adjacent to 4-cycles $B'_1B'_2F'B'_8$ and $B'_2F'B'_4B'_3$ (Fig. 11).

Let us show that none of these four patterns can be continued in order to design the embedding of the elongated dodecahedron. Indeed, for patterns (a), (b) and (d) in Fig. 11, edges $B'_7B'_8$ and $B'_1B'_8$ must be edges of the 6-cycle that is an image of face 1 [Fig. 8(a)]. Since these two edges belong to the same line, it can only be a 'one plane' 6-cycle. However, in this case, one more edge must be adjacent to the vertex B'_1. It is impossible, because this edge already has degree 3. A similar situation arises with pattern (c). Edges $B'_5B'_4$ and $B'_3B'_4$ must be the edges of the same 6-cycle that can only be the 'one plane' cycle. It implies that another edge must be adjacent to B'_3. This is impossible, since B'_3 already has degree 3.

We conclude that the 'one cube' 6-cycle with edges $B'_1B'_2$ and $B'_3B'_2$ as the image of the hexagonal face does not exist. Hence, it can only be the 'one plane' 6-cycle. As shown in Fig. 12, there are two possible ways to continue designing the embedding of the elongated dodecahedron using the 'one plane' 6-cycles.

Since both perpendicular planes with two pairs of the initial 4-cycles are equivalent, both ways to attach a 6-cycle as shown in Fig. 12 are also equivalent. Assume that the 6-cycle is adjacent as shown in Fig. 12(a) and let us refer again to Fig. 9 to continue the proof. First, with the already positioned 4- and 6-cycles, there is only one option to design the 6-cycle $B'_3B'_4B'_5A'_5A'_4A'_3$. Indeed, we have two edges $B'_3B'_4$ and $B'_5B'_4$ that belong to the same line; therefore, this 6-cycle is a 'one plane' cycle. The already designed edge $B'_3A'_3$ uniquely determines the plane for this 6-cycle.

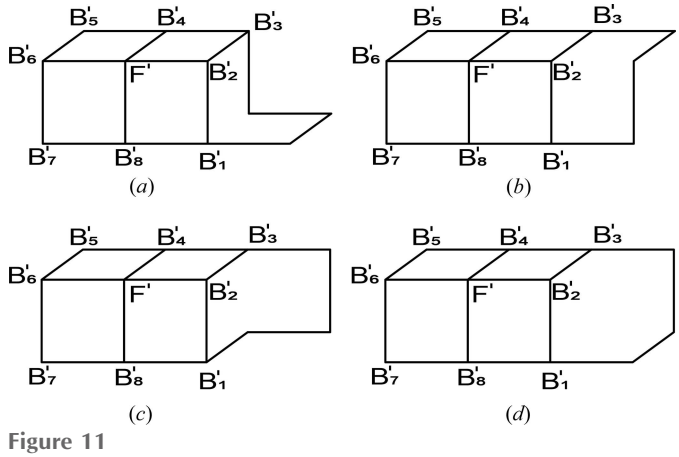

Figure 11
Four 'one cube' 6-cycles adjacent to 4-cycles $B'_1B'_2F'B'_8$ and $B'_2F'B'_4B'_3$.

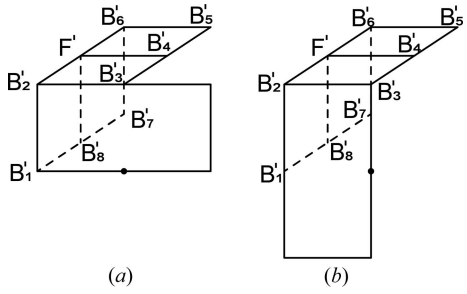

Figure 12
Two 'one plane' 6-cycles adjacent to 4-cycles $B'_1B'_2F'B'_8$ and $B'_2F'B'_4B'_3$.

Using the same argument for edges $B'_5B'_6$ and $B'_7B'_6$ we used for $B'_1B'_2$ and $B'_3B'_2$ to define $B'_1B'_2B'_3A'_3A'_2A'_1$, we can claim that the 6-cycle $B'_7B'_6B'_5A'_5A'_6A'_7$ is a 'one plane' cycle. Since the edge $B'_5A'_5$ of this cycle is already designed, we know the plane where this 6-cycle $B'_7B'_6B'_5A'_5A'_6A'_7$ is situated. Two 6-cycles $B'_1B'_2B'_3A'_3A'_2A'_1$ and $B'_7B'_6B'_5A'_5A'_6A'_7$ uniquely define the 6-cycle $B'_1B'_8B'_7A'_7A'_8A'_1$ and two 4-cycles $A'_1A'_8G'A'_2$ and $A'_8A'_7A'_6G'$. Finally, with the already designed cycles, two 4-cycles $A'_2A'_3A'_4G'$ and $A'_4A'_5A'_6G'$ are uniquely defined. As a result, we get a unique embedding as shown in Fig. 9. □

3.3. Embedding of a rhombic dodecahedron into a 4D pcu net

Theorem 3.6. A rhombic dodecahedron cannot be embedded into the 3D **pcu** net.

Proof. Let us take a rhombic dodecahedron (Fig. 13) and its vertex Y of degree 4. Assume there is an embedding of the rhombic dodecahedron into the **pcu** net. By Lemma 3.1 point (iii), four rhombic faces (*e.g.* faces 1, 2, 4, 5) can be mapped either onto four 4-cycles in one plane as shown in Fig. 3(*a*), or onto four 4-cycles in two perpendicular planes as shown in Fig. 3(*b*). In both cases, there are two 4-cycles that belong to the same plane. Assume these cycles are $1'$ (the image of 1) and $2'$ (the image of 2). Faces 1 and 2 have a common edge YS (with image $Y'S'$). Since $1'$ and $2'$ are on the same plane, the 4-cycle that has edges $Q'S'$ and $T'S'$ (4-cycle $3'$) cannot be adjacent to vertex S'. Hence, the rhombic dodecahedron cannot be embedded into the **pcu** net. □

Though the rhombic dodecahedron cannot be embedded into the **pcu** net, it is known that Theorem 3.7 below holds true. The constructions of the embedding of the rhombic dodecahedron and tiling by it are used in the next section to develop the SA representing the tiling by the rhombic dodecahedron.

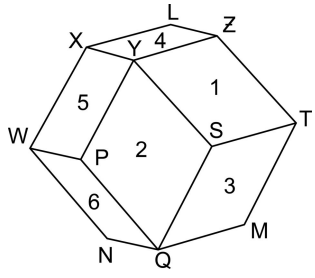

Figure 13
Rhombic dodecahedron.

Theorem 3.7. A rhombic dodecahedron and tiling by the rhombic dodecahedron can be embedded into the 4D **pcu** net (Definition 2.7 for $n = 4$).

Proof. Let us take the 4D unit cube $[0, 1]^4$ with the edge graph denoted by Γ. If we exclude vertices O, D' and edges incident to these vertices from Γ, we obtain the graph Γ_1 (Fig. 14). It is combinatorially equivalent to the graph of the rhombic dodecahedron, *i.e.* the rhombic dodecahedron can be embedded into the 4D **pcu** net.

Assume that point O is the origin of the 4D **pcu** net, the x axis is in the direction of vector $\vec{OA}$, the y axis is in the direction of vector $\vec{OB}$, the z axis is in the direction of vector $\vec{OC}$, and the upper part of the picture is a parallel shift along the t axis by the unit vector [0, 0, 0, 1]. Then, points marked without a 'prime' symbol have the following coordinates O = (0, 0, 0, 0), A = (1, 0, 0, 0), B = (0, 1, 0, 0), F = (1, 1, 0, 0), C = (0, 0, 1, 0), E = (1, 0, 1, 0), G = (0, 1, 1, 0), D = (1, 1, 1, 0). For all points that are marked with the 'prime' symbol, the fourth coordinate 1 is added to the coordinates of the corresponding points marked with the same letter without the 'prime' symbol.

To prove that tiling by the rhombic dodecahedron can be embedded into the 4D **pcu** net, let us introduce matrix

$$\mathbf{M} = \frac{1}{2}\begin{pmatrix} 1 & 1 & -1 & -1 \\ 1 & -1 & 1 & -1 \\ 1 & -1 & -1 & 1 \end{pmatrix}$$

that defines a linear mapping from $\mathbb{R}^4$ onto $\mathbb{R}^3$ ['projection' along the main diagonal of $[0, 1]^4$ that connects points (0, 0, 0, 0) and (1, 1, 1, 1)].

It is easy to check that $\mathbf{M}([0, 1]^4)$ is a rhombic dodecahedron. Let us denote it as P. **M** maps points O, D' onto the origin, and edges of $[0, 1]^4$ adjacent to O and D' are mapped inside P. Hence, **M** establishes isomorphism between Γ_1 and the edge graph of P. The inverse of this isomorphism is denoted by f. Since **M** is a linear mapping, then for any vector **v**

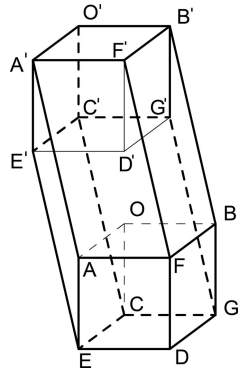

Figure 14
$[0, 1]^4$ and embedding of a rhombic dodecahedron into a 4D **pcu** net.

in $\mathbb{R}^4$ $\mathbf{M}([0,1]^4+\mathbf{v})=\mathbf{M}([0,1]^4)+\mathbf{M}(\mathbf{v})$. Vectors $e_1=[1,0,1]$, $e_2=[0,1,1]$ and $e_3=[-1,0,1]$ form a basis of the lattice Λ_P of tiling by P. Vectors $e_1'=[1,0,-1,0]$, $e_2'=[1,-1,0,0]$ and $e_3=[0,-1,0,1]$ such that $\mathbf{M}(e_i')=e_i$ $(i=1,2,3)$ form a basis for the lattice of embedding $\tilde{f}$ (extension of f) of tiling by P that can be defined in the following way. For any given integers λ_i $(i=1,2,3)$, the edge graph of a rhombic dodecahedron $P+\sum_1^3\lambda_i e_i$ maps by $\tilde{f}$ onto $f(P)+\sum_1^3\lambda_i e_i'$. It is easy to see that $\tilde{f}$ is well defined, *i.e.* for a vertex that belongs to adjacent cells, the image of this vertex is the same, irrespective of the cell to which it is considered to belong.

Let us note that the images of facet vectors under embedding $\tilde{f}$ shift centrally symmetric parallel 4-cycles in Γ_1 onto each other. For example, e_1' shifts $C'CGG'$ onto $A'AFF'$, e_2' shifts $B'BGG'$ onto $A'AEE'$, and e_3' shifts $FBGD$ onto $A'O'C'E'$. □

3.4. Embedding of a truncated octahedron into a pcu net

In this subsection, we will show that the truncated octahedron and tiling by the truncated octahedron can be embedded into the **pcu** net only in two different ways.

The image of the truncated octahedron obtained with the first method can be perceived as placed onto the surface of the $2\times2\times2$ cube in the **pcu** net with two cutout opposite corners. We call it a 'cutout corners' embedding.

The image developed with the second method can be perceived as placed onto the surface of the $2\times3\times1$ parallelepiped in the **pcu** net. We call this image a 'matchbox' ('matchbox' embedding). The same notations for the vertices of the truncated octahedron are used for both methods. Since the 'cutout corners' embedding is a more complicated construction, the notation of the vertices of the truncated octahedron (and the 'cutout corners' embedding) is chosen to make it easy to perceive this embedding. Namely, all nodes of the embedding at the lower base of the $2\times2\times2$ cube are denoted by letters A_i' $(i=1,\ldots9)$, by B_i' $(i=1,\ldots8)$ at the middle 'level', and by C_i' $(i=1,\ldots9)$ at the upper base such that A_i', B_i' and C_i' belong to the same line [Fig. 15(*b*)].

Theorem 3.8. A truncated octahedron can be embedded into the **pcu** net.

Proof. Method 1. The 'cutout corners' embedding. Let us take the $2\times2\times2$ cube in the **pcu** net as shown in Fig. 15(*b*). We indicate by bold lines the images of the truncated octahedron's edges under the suggested mapping.

For the 'cutout corners' method, we included more explanations than for other parallelohedra to substitute to some extent the proof of the theorem that the 'cutout corners' embedding is unique (Theorem 3.10).

Face 1 [Fig. 15(*a*)] of the truncated octahedron is mapped onto 6-cycle $B_8'C_8'C_9'C_6'B_6'B_7'$ in the $2\times2\times2$ cube. Face 2 is mapped onto $2'=A_7'B_7'B_6'B_5'A_5'A_6'$. Face 3 is mapped onto $3'=A_1'B_1'C_1'C_8'B_8'A_8'$.

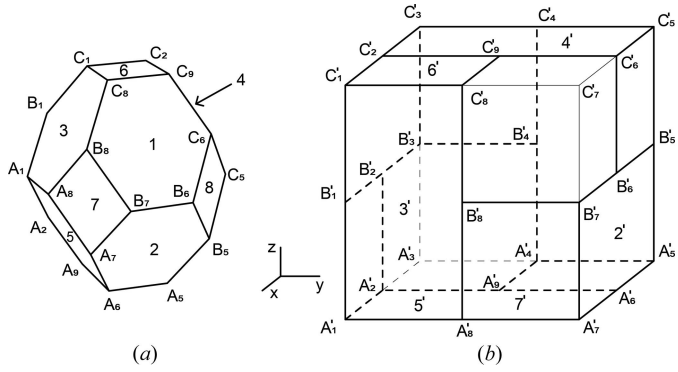

(*a*) (*b*)

Figure 15
'Cutout corners' embedding of a truncated octahedron.

There is one hexagonal face marked 4 in Fig. 15(*a*) that has a common edge with face 1. Face 4 is mapped onto $4'=C_2'C_3'C_4'C_5'C_6'C_9'$.

Face 1 also has three adjacent square faces, namely, faces 8, 7 and 6 as shown in Fig. 15(*a*). Face 8, besides being adjacent to 1, is also adjacent to hexagonal faces 2 and 4; therefore, $8'$ must have adjacent cycles $1'$, $2'$ and $4'$. This requirement determines $8'=B_6'C_6'C_5'B_5'$.

Square face 7, besides being adjacent to 1, is also adjacent to hexagonal faces 3 and 5; therefore, $7'$ must have adjacent cycles $1'$, $3'$ and $5'$. This requirement determines $7'=A_8'B_8'B_7'A_7'$ and $5'=A_1'A_2'A_9'A_6'A_7'A_8'$ such that $7'$ is adjacent to $1'$, $2'$, $3'$ and $5'$.

Square face 6 adjacent to 1 is also adjacent to hexagonal faces 4 and 3; therefore, $6'=C_1'C_2'C_9'C_8'$.

So far, we have mapped eight faces (with edges and vertices) of the truncated octahedron onto nodes and edges of the $2\times2\times2$ cube in the **pcu** net. To complete the embedding as shown in Fig. 15, we continue the mapping following the rule that the edge of the adjacent by the common edge faces in the truncated octahedron is mapped onto the adjacent by the common edge closed cycles of the $2\times2\times2$ cube.

Method 2. The 'matchbox' embedding. Let us take the $2\times3\times1$ parallelepiped P' in the **pcu** net as shown in Fig. 16(*b*). Here all marked lines indicate images of the truncated octahedron's edges under the suggested mapping. Fig. 16 is a self-explanatory picture that shows the construction of the 'matchbox' embedding on the assumption that all vertices A_i,

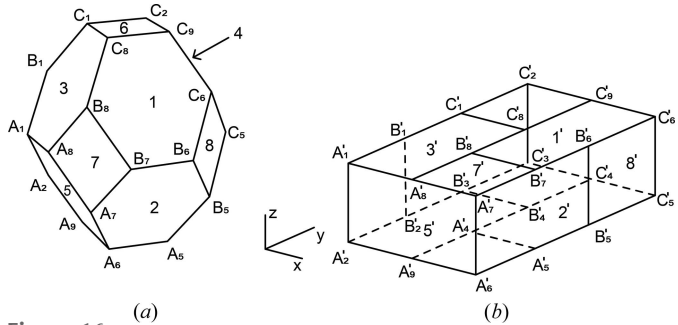

(*a*) (*b*)

Figure 16
'Matchbox' embedding of a truncated octahedron.

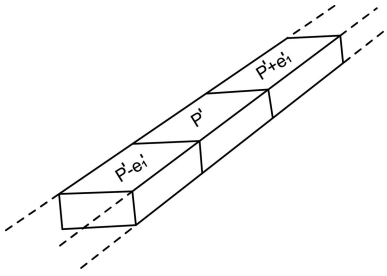

Figure 17
Truncated octahedron tiling embedding. Shift of P' by e'_1 along the y axis.

B_i, C_i of the truncated octahedron and edges that connect these vertices are mapped onto the corresponding vertices A'_i, B'_i, C'_i and the corresponding edges. □

Theorem 3.9. A tiling by the truncated octahedron can be embedded into the **pcu** net.

Proof. As follows from Remark 3.1, both embeddings of the truncated octahedron as described in the previous theorem can be extended to the embeddings of the tiling by the truncated octahedron. We discuss these embeddings in more detail below.

(i) 'Matchbox' embedding of tiling by the truncated octahedron. We introduce a system of coordinates and the origin in the **pcu** net. Let A'_2 be the origin (0, 0, 0) (Fig. 16), the x axis is along the edge $A'_2A'_6$, the y axis is along the edge $A'_2C'_3$ and the z axis is along the edge $A'_2A'_1$.

The following vectors form the basis for Λ_P: $e_1 = \vec{A_2C_3}$ corresponding to face 5 and parallel to it face 4; $e_2 = \vec{B_1A_7}$ (face 2 and face ∥ 2); and $e_3 = \vec{B_4A_7}$ (face ∥ 7 and face 7).

The corresponding vectors that form the basis for $\Lambda'_{f(P)}$ are vectors: $e'_1 = \vec{A'_2C'_3} = [(0, 3, 0) - (0, 0, 0)] = [0, 3, 0]$;

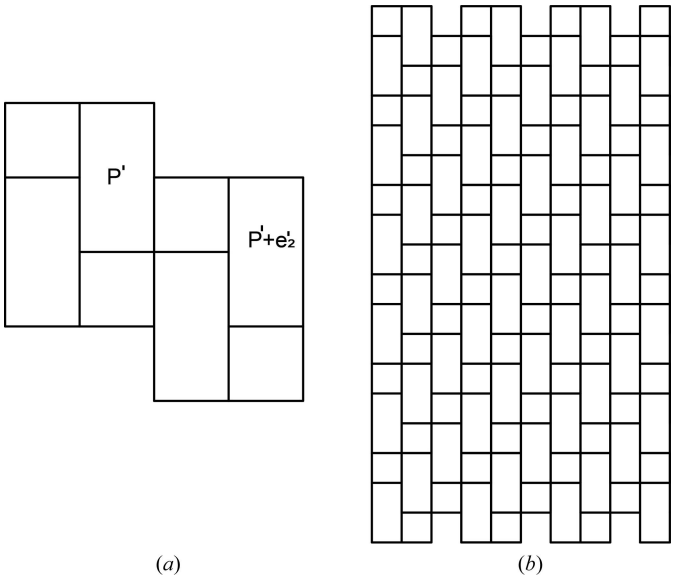

(*a*) (*b*)

Figure 18
(*a*) Projection of shift of P' by e'_2. (*b*) Projection of strips that occur as shifts by multiples of e'_2.

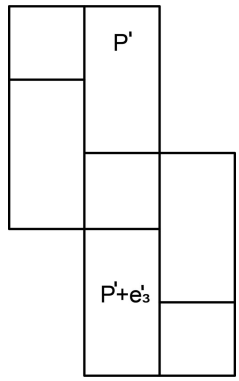

Figure 19
Truncated octahedron tiling embedding. Projection of shift of P' by e_3.

$e'_2 = \vec{B'_1A'_7} = [(2, 0, 1) - (0, 1, 1)] = [2, -1, 0]$; and $e'_3 = \vec{B'_4A'_7} = [(2, 0, 1) - (1, 2, 0)] = [1, -2, 1]$.

By adding to P' all vectors that are multiples with integer coefficients of e'_1, we develop an infinite strip in the **pcu** net of copies of P' in the direction of the y axis as shown in Fig. 17. We show the projection of shifting P' by e'_2 on plane $z = 0$ in Fig. 18(*a*). P' and $P' + e'_2$ are at the same horizontal level. To illustrate how the embedding is constructed, we develop five strips of tiling that are the result of shifts of the above-designed strip by multiples with integer coefficients of e'_2. The projection of these five strips on the plane $z = 0$ is shown in Fig. 18(*b*). The projection of the shift of P' by e_3 is shown in Fig. 19. P' is one unit lower than $P' + e'_3$.

All parallel and centrally symmetric around the center of P' cycles that are images of the truncated octahedron can be moved onto each other by adding a linear combination with integer coefficients of e'_1, e'_2 and e'_3 to the corresponding parallel cycle.

For example, cycle $A'_2B'_2B'_3B'_4A'_4A'_9$ is shifted onto cycle $1' = B'_8C'_8C'_9C'_6B'_6B'_7$ by vector $e'_4 = \vec{A'_2B'_8} = [(1, 1, 1) - (0, 0, 0)] = [1, 1, 1] = e'_1 + e'_3$. The result of the shift is demonstrated in Fig. 20.

(ii) 'Cutout corners' embedding of tiling by the truncated octahedron. It is convenient to keep the same origin in the **pcu** net as in the previous case but choose different directions for the x axis, y axis and z axis. Let A'_2 be the origin (0, 0, 0) [Fig. 15(*b*)], the x axis is along the edge $A'_2A'_1$, the y axis is along the edge $A'_2A'_6$ and the z axis is along the edge $A'_2B'_2$. Unlike the previous case, where all images of hexagonal faces are 'one plane' embeddings, faces 1 and ∥ 1 are embedded as a 'hexagon shape'. This is the reason to choose a different basis of Λ_P.

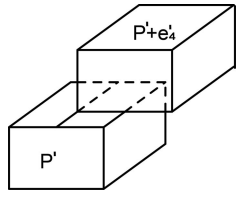

Figure 20
Truncated octahedron tiling embedding. Shift of P' by e_4.

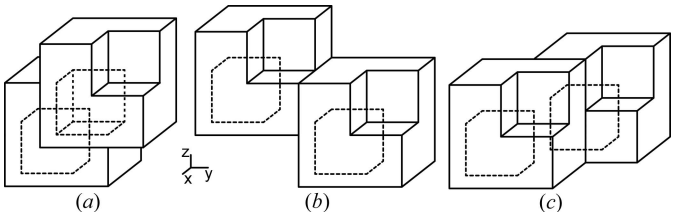

Figure 21
P' and shift of P' by: (*a*) e'_1, (*b*) e'_2, (*c*) e'_3.

The facet vector $e_1 = \vec{A_2B_8}$ that shifts face ∥ 1 onto face 1 is the first vector of the basis of Λ_P. The corresponding vector for the basis of $\Lambda'_{g(P)}$ (g stands for the 'cutout corners' embedding) is vector $e'_1 = [1, 1, 1]$. We choose two other vectors for the basis of Λ_P to be $e_2 = \vec{B_2A_6}$ (shifts face ∥ 2 onto face 2) and $e_3 = \vec{A_4A_1}$ (shifts face ∥ 3 onto face 3). The corresponding vectors for the basis of $\Lambda'_{g(P)}$ are $e'_2 = [0, 2, -1]$ and $e'_3 = [2, -1, 0]$.

We show fragments of the 'cutout corners' tiling embedding in Fig. 21. □

Below are the outlines of proofs of several theorems from which it follows that there are only two ways to embed the truncated octahedron as described above.

Theorem 3.10. If, in the embedding of the truncated octahedron into the **pcu** net, one of the images of a hexagonal face is the 'hexagon shape' 6-cycle, then the embedding is uniquely defined by the 'hexagon shape' 6-cycle. It does not contain any 'angle shape' 6-cycles, *i.e.* only 'one plane' or 'hexagon shape' 6-cycles can be the image of a hexagonal face of the truncated octahedron.

Proof. The proof is a step-by-step construction of the images of the truncated octahedron faces starting with the 'hexagon shape' 6-cycle. As the result, we obtain, uniquely defined by the initial choice of the 'hexagon shape', the 6-cycle embedding as shown in Fig. 15. We omit the details of this lengthy proof. Several options to attach the 6-cycle or 4-cycle are considered at every step. We show that only one of these options reflects a combinatorial structure of the truncated octahedron and does not lead to a dead end in the construction. □

Theorem 3.11. For any embedding of the truncated octahedron into the **pcu** net, the 'angle shape' 6-cycle is not the image of any hexagonal face of the truncated octahedron, *i.e.* only 'one plane' or 'hexagon shape' 6-cycles can be the image of a hexagonal face of the truncated octahedron under any embedding into the **pcu** net.

Proof. The technique of this proof is similar to that of Theorem 3.10. □

Theorem 3.12. The embedding of the truncated octahedron into the **pcu** net is uniquely defined, provided the 'hexagon shape' 6-cycle is not the image of any hexagonal face. It is a 'matchbox' embedding as constructed in Theorem 3.8 with Method 2.

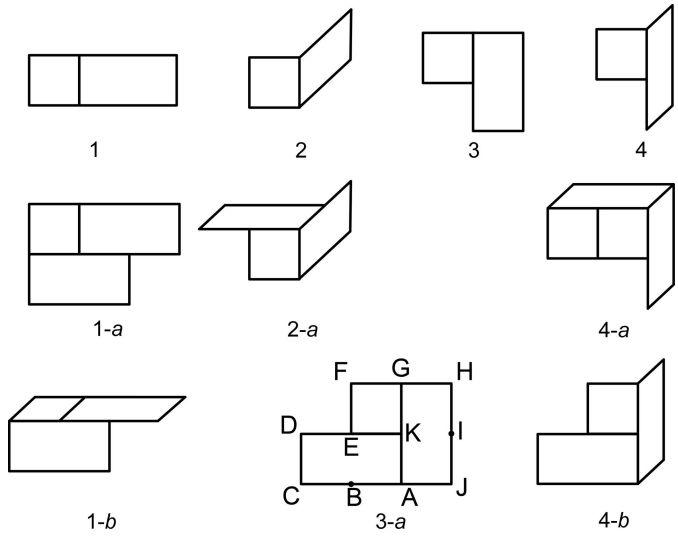

Figure 22
Row I: four ways to attach a 4-cycle and 'one plane' 6-cycle along the common edge; rows II, III: six ways to attach two 'one plane' 6-cycles and one 4-cycle.

Proof. We provide a brief sketch of the proof below.

(i) It is easy to see that, up to symmetry, there are four different ways to attach a 4-cycle and the 'one plane' 6-cycle along the common edge. We listed all these patterns in the first row of Fig. 22. In the second and third rows, we show six possible ways to arrange two 'one plane' 6-cycles and one 4-cycle such that these arrangements preserve the structure of the truncated octahedron. We did not include equivalent patterns that could be obtained in different ways in Fig. 22.

Note that the pattern shown in Fig. 22(3-*a*) cannot be continued to the embedding of the truncated octahedron.

Indeed, let us take vertex A that is already the vertex of two adjacent 6-cycles and has degree 3. A must also be a vertex of the 4-cycle that is the image of a face of the truncated octahedron. Since no new edges can be adjacent to A, two out of

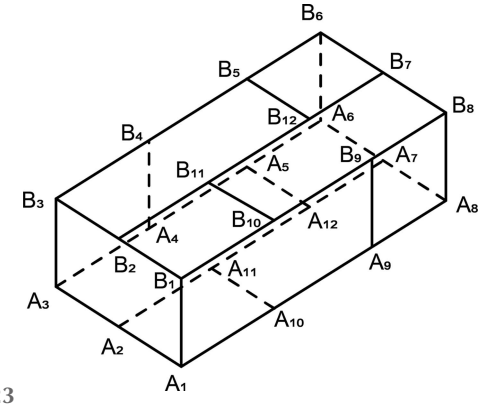

Figure 23
Restoring 'matchbox' embedding from pattern (2-*a*).

three edges BA, JA, KA must be the edges of the new 4-cycle adjacent to A. Since KA is already an edge of two 6-cycles, it cannot be KA. At the same time, BA and JA belong to the same line, hence there is no 4-cycle with these two edges.

In most cases, starting with patterns from Fig. 22 [(1-*a*) to (4-*b*) excluding (3-*a*)], it is clear how the next cycle can be adjacent to the vertex under consideration. If it cannot be done, then the argument and the pattern when it cannot be done are the same as in the previous case. For this reason, we discuss only two more cases, listing them in the order in which the cycles are constructed. We add in parentheses the vertex to which the new cycle is adjacent.

The first case is (2-*a*), when at each step there is only one option to construct the next cycle.

Let us take the (2-*a*) pattern $A_8A_9B_9B_{10}B_{11}B_{12}B_7B_6A_6A_7$ as shown in Fig. 23.

$A_8A_9B_9B_{10}B_{11}B_{12}B_7B_6A_6A_7 \Rightarrow (A_8)$ - $A_8A_9A_{10}A_{11}A_{12}A_7$ and (B_7) - $B_7B_{12}B_5B_6 \Rightarrow (A_9)$ - $A_9A_{10}A_1B_1B_{10}B_9$ and (A_7) - $A_7A_{12}A_5A_6 \Rightarrow (B_{10})$ - $B_{10}B_1B_2B_{11}$ and (A_{10}) - $A_{10}A_1A_2A_{11} \Rightarrow (B_{11})$ - $B_{11}B_2B_3B_4B_5B_{12}$ and (A_{11}) - $A_{11}A_2A_3A_4A_5A_{12} \Rightarrow (A_6)$ - $A_6A_5A_4B_4B_5B_6$ and (A_1) - $A_1A_2A_3B_3B_2B_1 \Rightarrow (A_4)$ - $A_4A_3B_3A_4$.

In a similar way, we show that patterns (1-*a*), (1-*b*), (4-*a*) and (4-*b*) in Fig. 22 can be completed to become the embedding of the truncated octahedron.

For patterns (1-*b*) and (4-*a*), there are two different options to proceed at some step. In any of the cases (1-*a*), (1-*b*), (2-*a*), (4-*a*) and (4-*b*) the final construction will be a 'matchbox' embedding. □

For all patterns listed in rows two and three of Fig. 22 [except patterns (1-*b*), (4-*a*) and (3-*a*)], every next step is uniquely determined by the previous steps of constructing the embedding without the 'hexagon shape' 6-cycle.

Now we formulate the last theorem of the subsection that immediately follows from all the theorems discussed above.

Theorem 3.13. There are two and only two embeddings of the truncated octahedron into the **pcu** net. One contains only 'one plane' 6-cycles and 4-cycles; the second contains only two 'hexagon shape' 6-cycles, 'one plane' 6-cycles and 4-cycles. Both embeddings do not contain 'angle shape' 6-cycles.

4. SA representation of the tiling by a parallelohedron

The main objective of this section is to construct SA that represent the edge graphs of tilings by parallelohedra. The SA that represents a given tiling by the parallelohedron accepts words that correspond to the paths in the edge graph of the embedding (and, therefore, of the tiling itself) and rejects words that do not.

4.1. DFA and SA

In this subsection, we briefly discuss the definition of the DFA and the SA as an example of a DFA. Here we follow the work of Krivovichev (2014*a*) and Hopcroft *et al.* (2001).

As defined by Hopcroft *et al.* (2001), DFA $\mathcal{A}$ consists of five components, *i.e.* $\mathcal{A} = (\mathbf{Q}, \mathbf{\Sigma}, \boldsymbol{\delta}, \mathbf{q}_1, \mathbf{F})$ where $\mathbf{Q} = \{\mathbf{1}, \mathbf{2}, \mathbf{3}, \mathbf{4} \ldots \mathbf{n}\}$ is a finite set of states; $\mathbf{\Sigma}$ is a finite set of transitional or input symbols; $\boldsymbol{\delta}$ is a transition function of two arguments (state and input symbol); the value of $\boldsymbol{\delta}$ is a new state; $\mathbf{q}_1$ is an initial or start state; $\mathbf{F}$ is a set of final or accepting states. The set $\mathbf{F}$ is a subset of $\mathbf{Q}$.

The set of input symbols is called an alphabet. The sequence of input symbols is a word or a string. We describe how the DFA processes strings and decides whether to accept a sequence of input symbols (Hopcroft *et al.*, 2001). Let us take a word $\mathbf{a}_1 \ldots \mathbf{a}_n$ and the start state $\mathbf{q}_1$. By finding the value $\boldsymbol{\delta}(\mathbf{q}_1, \mathbf{a}_1) = \mathbf{q}_2$ of the transition function $\boldsymbol{\delta}$, the automaton processes the first input symbol $\mathbf{a}_1$. The second symbol $\mathbf{a}_2$ is processed by evaluating $\boldsymbol{\delta}(\mathbf{q}_2, \mathbf{a}_2)$ and obtaining the new state $\mathbf{q}_3$. The automaton continues in this manner finding states $\mathbf{q}_1 \ldots \mathbf{q}_n$ such that $\boldsymbol{\delta}(\mathbf{q}_i, \mathbf{a}_i) = \mathbf{q}_{i+1}$ for each i $(1 \leq i \leq n)$. If $\mathbf{q}_{n+1} \in \mathbf{F}$, then the string $\mathbf{a}_1 \ldots \mathbf{a}_n$ is accepted by $\mathcal{A}$, and if $\mathbf{q}_{n+1} \notin \mathbf{F}$, the string $\mathbf{a}_1 \ldots \mathbf{a}_n$ is not accepted (rejected).

Note that, by the definition of the DFA, the domain of the function $\boldsymbol{\delta}$ is the set $\mathbf{Q} \times \mathbf{\Sigma}$. This finite automaton is called a complete DFA. However, for problems related to modeling crystalline structures and other areas, a slightly different notion is used by some authors, like in the work of Morey *et al.* (2002). The transition function is defined on a subset of $\mathbf{Q} \times \mathbf{\Sigma}$, and this type of DFA is called a partial DFA. When no transition is defined, the automaton halts. Since we consider only partial DFA where $\mathbf{Q} = \mathbf{F}$, assume for simplicity that $\mathbf{Q} = \mathbf{F}$ in the definition of the accepted strings for a partial DFA. In this case, a word $\mathbf{a}_1 \ldots \mathbf{a}_n$ is accepted if and only if $\boldsymbol{\delta}(\mathbf{q}_i, \mathbf{a}_i)$ is defined for each i $(1 \leq i \leq n)$, *i.e.* the automaton does not halt.

There are two efficient ways to describe the structure of a DFA: as a state diagram where vertices are states and edges are input symbols; and as a transition table (matrix) where labels of rows are states, labels of columns are input symbols, and an intersection is a value of function $\boldsymbol{\delta}$.

If $\mathbf{W}$ is a set of all words that DFA $\mathcal{A}$ accepts, we call $\mathbf{W} = L(\mathcal{A})$ a formal language of DFA $\mathcal{A}$, or we say that $\mathcal{A}$ recognizes $\mathbf{W}$. Note that $\mathcal{A}$ generates $\mathbf{W}$ by listing all possible pathways of changing states. The production rules (formal grammar) for the words from $L(\mathcal{A})$ are defined as a state diagram or a transition matrix. If a DFA recognizes all possible words from a given alphabet, it is called a universal automaton $\mathcal{A}_U$ for the given alphabet.

In Fig. 24, we give a self-explanatory example of these two ways to represent a DFA with a partially defined transition matrix and $\mathbf{Q} = \mathbf{F}$. The DFA with a partially defined transition function accepts **abcbc** and **bcccbc**, though it rejects **aba** or **bbc** strings.

Two finite automata are considered equivalent if they have the same alphabet and accept the same set of strings, *i.e.* have the same language.

Using the example of partial DFA $\mathcal{A}$ defined in Fig. 24, we will demonstrate how to construct a complete DFA that is equivalent to the given partial DFA. Assume the set of states $\mathbf{Q}'$ for complete DFA $\mathcal{A}'$ is obtained from the set of states $\mathbf{Q}$ of

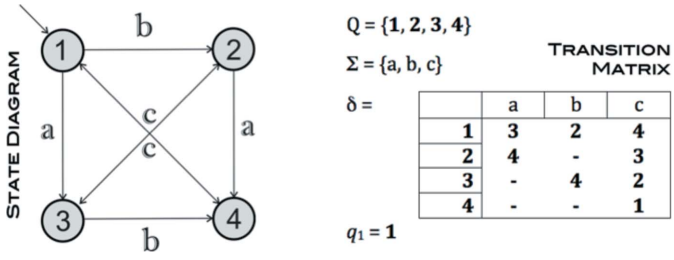

	a	b	c
1	3	2	4
2	4	-	3
3	-	4	2
4	-	-	1

Figure 24
Example of a DFA (Krivovichev, 2014*a*).

partial $\mathcal{A}$ by adding just one state that will be denoted by the symbol '-', *i.e.* $\mathbf{Q}' = \mathbf{Q} \cup \{\text{'-'}\}$. Let us take the transition matrix for $\mathcal{A}$ as shown in Fig. 24 and add to this matrix another row at the bottom that consists of five symbols '-'. This new transition matrix determines the transition function $\boldsymbol{\delta}$ with the domain $\mathbf{Q}' \times \boldsymbol{\Sigma}$ for the complete DFA $\mathcal{A}'$. $\mathbf{Q}$ is a set of accepting states for $\mathcal{A}'$. It is easy to show that the finite automata $\mathcal{A}'$ and $\mathcal{A}$ are equivalent. We used this example to demonstrate how to construct an equivalent complete DFA for a given partial DFA. A similar construction can be done for any partial DFA. In particular, it can be constructed for any SA that will be defined and discussed below.

For the description of crystal growth, Shevchenko *et al.* (2008) and Krivovichev *et al.* (2012) suggested using a partial DFA called structural automata or crystal structure automata. The concept was introduced by Morey *et al.* (2002). In SA, each state is a class of equivalent vertices in the **pcu** net with a certain configuration of edges incident to each vertex (class of vertices). The set of symbols $\boldsymbol{\Sigma}$ of an SA is defined as a set of vectors of length 1 incident to the fixed vertex in the nD **pcu** net or directed edges that indicate directions in the **pcu** net. The transition function identifies a transition from state $\mathbf{q}_i$ to state $\mathbf{q}_j$ via the vector $\mathbf{v}$ that belongs to the set $\boldsymbol{\Sigma}$: $\boldsymbol{\delta}(\mathbf{q}_i, \mathbf{v}) = \mathbf{q}_j$. For each vector $\mathbf{v}$ in $\boldsymbol{\Sigma}$, there is an opposite vector $\underline{\mathbf{v}}$, *i.e.* an SA is a bi-directional automaton. Any state (vertex) from $\mathbf{Q}$ may be an initial state, and any state from $\mathbf{Q}$ is an accepting state. This definition can be extended to the nD **pcu** net. Unless specified differently, it is assumed that $n = 3$.

The simplest example of SA construction is related to the **pcu** net itself. As we have already noted, the **pcu** net can be defined as $\mathbb{Z}^3$ where all nodes are connected by unit edges, *i.e.* for every node there are six orthogonal edges that connect this node with the adjacent ones. Vectors in $\boldsymbol{\Sigma}$ = {**a**, $\underline{\mathbf{a}}$, **b**, $\underline{\mathbf{b}}$, **c**, $\underline{\mathbf{c}}$} constitute a standard orthonormal basis for $\mathbb{R}^3$ plus their opposite vectors. The diagram for the SA that generates the **pcu** net is very simple: a one vertex state. There is only one edge configuration for every vertex with six loops {**a**, $\underline{\mathbf{a}}$, **b**, $\underline{\mathbf{b}}$, **c**, $\underline{\mathbf{c}}$}, and all vertices are equivalent (Fig. 25). Using the language of the SA, we say that all words formed in the alphabet $\boldsymbol{\Sigma}$ = {**a**, $\underline{\mathbf{a}}$, **b**, $\underline{\mathbf{b}}$, **c**, $\underline{\mathbf{c}}$} are accepted. Hence, the SA that represents the **pcu** net is a universal automaton.

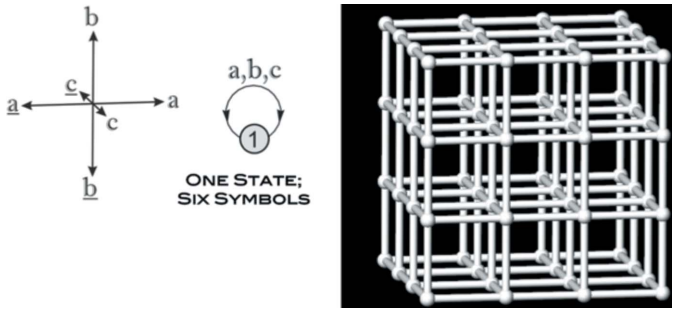

Figure 25
pcu net as the universal language of the SA (Krivovichev, 2014*a*).

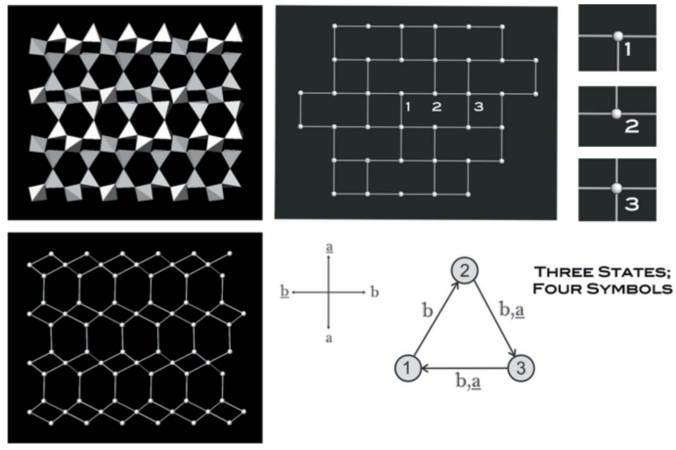

Figure 26
Tetrahedral layer in the structure of RUB-15 (upper left), its nodal (lower left) and orthogonal (upper central) representations. The orthogonal network contains three different vertex configurations (upper right). The central lower part shows the state diagram of the respective DFA. Modified after Krivovichev (2014*a*).

As another example of an SA besides the **pcu** net, we show the structure of RUB-15. The tetrahedral layer in the structure of RUB-15, its nodal and orthogonal representation (embedding into the **pcu** net) as well as three different configurations of edges at vertices that this network contains are shown in Fig. 26. The state diagram and the transition matrix for the SA representation of RUB-15 are shown in Fig. 27.

We would like to note that while discussing the embedding of the tiling by the truncated octahedron, we obtained the orthogonal network of RUB-15 [Fig. 18(*b*)] in the plane $z = 0$.

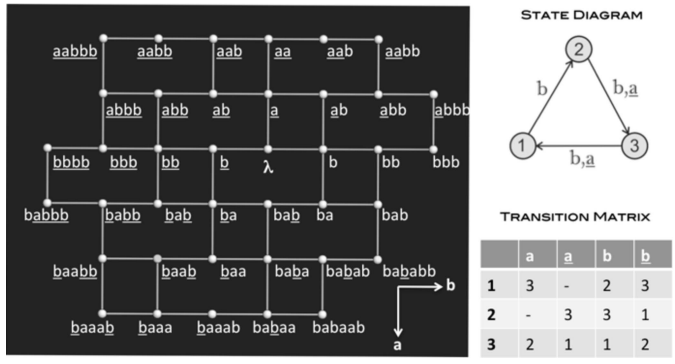

	a	a	b	b
1	3	-	2	3
2	-	3	3	1
3	2	1	1	2

Figure 27
The orthogonal version of the RUB-15 2D network with words assigned to the vertices (left), its state diagram (upper right) and transition matrix (lower right). Modified after Krivovichev (2014*a*).

Table 1
SA for a tiling by a hexagonal prism.

State	**a**	**a̲**	**b**	**b̲**	**c**	**c̲**
1	-	2	2	2	1	1
2	1	-	1	1	2	2

Table 2
SA for a tiling by an elongated dodecahedron.

State	**a**	**a̲**	**b**	**b̲**	**c**	**c̲**
1	2	2	3	3	-	4
2	1	1	4	4	-	-
3	4	4	1	1	-	-
4	3	3	2	2	1	-

4.2. SA representation of face-to-face tiling by a parallelohedron

In this subsection, we develop the SA that represents the embedding and serves as a model for the corresponding crystal growth for each tiling by the parallelohedron. Though the rhombic dodecahedron cannot be embedded into the 3D **pcu** net, we suggest using the embedding into the 4D **pcu** net (as designed in the previous section) to construct the SA representing the elongated dodecahedron.

Since the embedding of face-to-face tiling by the cube is the **pcu** net itself, the universal SA as described in Fig. 25 represents face-to-face tiling by the cube.

For simplicity, we adopted the concept of SA to construct the DFA representing tilings by parallelohedra, though, generally speaking, the SA is a partial DFA. Each SA is constructed by identifying **Q** with equivalence classes of transitionally equivalent vertices of the tiling with a certain configuration of incident edges. We denote elements of **Q** by natural numbers. For the hexagonal prism, elongated dodecahedron and truncated octahedron, **Σ** is a set of vectors that form an orthonormal basis in the **pcu** net plus their opposite vectors, *i.e.* **Σ** = {**a**, **a̲**, **b**, **b̲**, **c**, **c̲**}. In the case of the rhombic dodecahedron, the set **Σ** consists of four unit vectors that form an orthonormal basis in the 4D **pcu** net plus their opposite vectors, *i.e.* **Σ** = {**a**, **a̲**, **b**, **b̲**, **c**, **c̲**, **d**, **d̲**}. For **n** ∈ **Q** and **v** ∈ **Σ**, ***δ***(**n**, **v**) is an equivalence class adjacent to **n** in the direction of **v**, provided (**v**) represents a directed edge of the edge graph of the embedding. The set of the accepting states is equal to **Q**. Any state can be taken as the initial state.

For each parallelohedron, Tables 1–4 represent a tiling by a given parallelohedron. As we have already noted, a complete DFA equivalent to an SA can be constructed by adding a single non-accepting state '-' to **Q**. Hence, if we add an additional row of symbols '-' to each of the Tables 1–4, we will construct transition tables that define complete DFA equivalent to corresponding SA. To have a better understanding why the transition function is defined or not defined on some pairs of the state and input symbol, we demonstrate what a configuration of edges for each element from **Q** is, *i.e.* in which directions incident edges exist for a given class of equivalent vertices. In the SA constructed for each parallelohedron below, any state can be taken as the initial state.

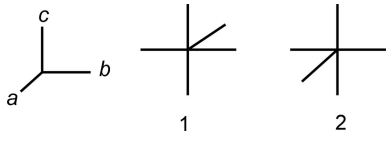

Figure 28
States' configurations for tiling by a hexagonal prism.

Table 3
SA for a tiling by a truncated octahedron.

State	**a**	**a̲**	**b**	**b̲**	**c**	**c̲**
1	-	2	4	3	-	6
2	1	3	5	6	-	-
3	2	-	1	4	-	5
4	6	5	3	1	-	-
5	4	-	6	2	3	-
6	-	4	2	5	1	-

Table 4
SA for a tiling by a rhombic dodecahedron.

State	**a**	**a̲**	**b**	**b̲**	**c**	**c̲**	**d**	**d̲**
1	2	-	2	-	2	-	2	-
2	3	1	3	1	3	1	3	1
3	-	2	-	2	-	2	-	2

There are two states in **Q** for the embedding of tiling by the hexagonal prism constructed in Theorem 3.1. Table 1 defines the SA that represents this tiling. Configurations of edges are shown in Fig. 28.

There are four states in **Q** for the embedding of tiling by the elongated dodecahedron constructed in Theorems 3.3 (Method 1) and 3.4. Table 2 defines the SA that represents this tiling. Configurations of edges are shown in Fig. 29.

There are six states in **Q** for the embedding of tiling by the truncated octahedron constructed in Theorems 3.8 and 3.9. Table 3 defines the SA that represents this tiling. Configurations of edges are shown in Fig. 30.

There are three states in **Q** for the embedding of tiling by the rhombic dodecahedron constructed in Theorem 3.7. Table 4 defines the SA that represents this tiling. Since we embedded

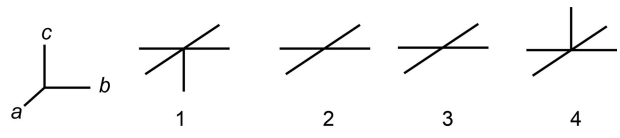

Figure 29
States' configurations for tiling by an elongated dodecahedron.

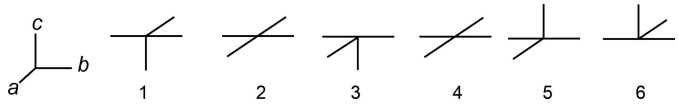

Figure 30
States' configurations for tiling by a truncated octahedron.

tiling by the rhombic dodecahedron into the 4D **pcu** net, we give the description for the configuration of edges at every class of equivalent vertices: state 1: **abcd**; state 2: **abbccdd**; state 3: **abcd**.

5. Summary

The analysis of the embeddings of tilings of 3D Euclidean space by Fedorov parallelohedra into the **pcu** net shows that the edge graphs of four out of five tilings are orthogonal in 3D, whereas the fifth one (tiling by the rhombic dodecahedron) is non-orthogonal in 3D, but orthogonal in 4D. If we define the complexity of the SA as the number of its states, tiling by the cube (the **pcu** net itself) is the simplest one containing one state only. Tiling by the hexagonal prism is the second in simplicity (two states), tiling by the elongated dodecahedron is the third (four states), whereas tiling by the truncated octahedron is the fourth (six states). Tiling by the rhombic dodecahedron cannot be compared directly with the other four, since it is orthogonal in a 4D but not in a 3D space. This raises an interesting question of comparative complexity measures for the nets existing in spaces of different dimensionalities. This methodological topic requires further exploration.

The advantage of using orthogonal nets in crystal growth models is that their SA can easily be programmed as existing on a cubic lattice. In the future, one may ask the following questions: (i) How many different SA exist in $\mathbb{R}^3$ with two, three, four and five states? (ii) How are these automata related to the existing topologies? (iii) Is there any correlation between the SA complexity and the occurrence of respective nets in real structures (inorganic and metal–organic)? (iv) Does combinatorial topological symmetry have an influence upon the occurrence of the algorithmically simplest nets? It is our intention to elaborate on these questions in the near future.

Acknowledgements

We greatly appreciate lengthy discussions about embeddings of parallelohedra with N. P. Dolbilin and M. I. Stogrin (Steklov Mathematics Institute of the Russian Academy of Sciences), their input, suggestions and advice at all stages of the preparation of this paper. We greatly appreciate the opportunity to meet at the workshop 'Soft Packings, Nested Clusters and Condensed Matter' hosted by the American Institute of Mathematics (AIM) where our collaboration started, and we are grateful to the organizers of the workshop and AIM for its hospitality. We would like to express our sincere gratitude to the referees for their thorough review of the paper and making valuable suggestions for improving it.

Funding information

SVK thanks the Russian Science Foundation for financial support (grant 19-17-00038).

References

Adar, R., Benenson, Y., Linshiz, G., Rosner, A., Tishby, N. & Shapiro, E. (2004). *Proc. Natl Acad. Sci. USA*, **101**, 9960–9965.
Alexandrov, E. V., Blatov, V. A., Kochetkov, A. V. & Proserpio, D. M. (2011). *CrystEngComm*, **13**, 3947–3958.
Baburin, I. A., Bouniaev, M., Dolbilin, N., Erokhovets, N. Y., Garber, A., Krivovichev, S. V. & Schulte, E. (2018). *Acta Cryst.* A**74**, 616–629.
Cartwright, J. H. E. & Mackay, A. L. (2012). *Proc. R. Soc. London Ser. A*, **370**, 2807–2822.
Coxeter, H. S. M. (1973). *Regular Polytopes*, 3rd ed. New York: Dover.
Crutchfield, J. P. (2012). *Nat. Phys.* **8**, 17–24.
Delgado Friedrichs, O., O'Keeffe, M. & Yaghi, O. M. (2003). *Acta Cryst.* A**59**, 22–27.
Delone, B. N., Dolbilin, N. P., Shtogrin, M. I. & Galiulin, R. V. (1976). *Dokl. AN SSSR*, **227**, 19–21.
Dolbilin, N. & Schattschneider, D. (1998). *Quasicrystals and Discrete Geometry. Fields Institute Monographs*, Vol. 10, pp. 193–199. Providence, Rhode Island, USA: American Mathematical Society.
Dolbilin, N. P. (1976). *Dokl. AN SSSR*, **230**, 516–519.
Dolbilin, N. P. (2012). *Tr. Mosk. Mater. Obshch.* **73**, 259–276.
Fedorov, E. S. (1885). *Elements of the Theory of Figures. Zap. Imp. Miner. Obsch.* **21**, 1–279.
Hopcroft, J. E., Morwani, R. & Ullman, J. D. (2001). *Introduction to Automata Theory, Languages and Computation*. Boston, USA: Addison-Wesley.
Hornfeck, W. (2020). *Acta Cryst.* A**76**, 534–548.
Krivovichev, S. V. (2004). *Acta Cryst.* A**60**, 257–262.
Krivovichev, S. V. (2009). *Structural Crystallography of Inorganic Oxysalts*. Oxford University Press.
Krivovichev, S. V. (2012). *Acta Cryst.* A**68**, 393–398.
Krivovichev, S. V. (2014*a*). *Miner. Mag.* **78**, 415–435.
Krivovichev, S. V. (2014*b*). *Angew. Chem. Int. Ed.* **53**, 654–661.
Krivovichev, S. V., Shcherbakova, E. P. & Nishanbaev, T. P. (2012). *Can. Mineral.* **50**, 585–592.
Mackay, A. L. (1976). *Phys. Bull.* **27**, 495–497.
Minkovski, H. (1897). *Nachr. Ges. Wiss. Gött.* pp. 198–287.
Morey, J., Sedig, K., Mercer, R. E. & Wilson, W. (2002). *Lecture Notes in Computer Sciences*, Vol. 2494, edited by B. W. Watson & D. Wood, pp. 214–222. Berlin: Springer-Verlag.
Schattschneider, D. & Dolbilin, N. (1998). *Quasicrystals and Discrete Geometry*. *Fields Institute Monographs*, Vol. 10, pp. 207–246. Providence, Rhode Island, USA: American Mathematical Society.
Shevchenko, V. Ya., Krivovichev, S. V. & Mackay, A. (2008). *Glass Phys. Chem.* **36**, 1–9.
Varn, D. P., Canright, G. S. & Crutchfield, J. P. (2013*a*). *Acta Cryst.* A**69**, 197–206.
Varn, D. P., Canright, G. S. & Crutchfield, J. P. (2013*b*). *Acta Cryst.* A**69**, 413–426.